Hindawi
Geofluids
Volume 2023, Article ID 7013843, 14 pages
https://doi.org/10.1155/2023/7013843

Research Article

Micropore Throat Structure and Movable Fluid Characteristics of Chang 6_3 Tight Sandstone in Baibao Area of Ordos Basin

Bobiao Liu,[1,2] **Chengqian Tan**,[1,2] **Yinchao Huai**,[1,2] **Nan Wang**,[3] **Han Zhang**,[1,2] **and Zhao Feng**[1,2]

[1]*School of Earth Science and Engineering, Xi'an Shiyou University, Xi'an 710065, China*
[2]*Shaanxi Key Laboratory of Petroleum Accumulation Geology, Xi'an Shiyou University, China*
[3]*Changqing Oilfield Branch No. 8 Oil Production Plant Geology Institute, Xi'an 710021, China*

Correspondence should be addressed to Yinchao Huai; huaiyinchao@xsyu.edu.cn

Received 7 December 2022; Revised 4 May 2023; Accepted 25 May 2023; Published 14 June 2023

Academic Editor: Bangsheng Zhao

Tight sand is an important unconventional reservoir. Aiming at the problem of large unused reserves and the poor development effect of Chang 6_3 reservoir, this paper researches reunderstanding reservoir and evaluating unused reserves. Employing rock slice and scanning electron microscope (SEM), the experiment of low-field nuclear magnetic resonance (NMR), water-oil relative permeability experiment, reservoir space, movable fluid, and oil-water seepage characteristics was studied. The factors affecting NMR T_2 cutoff, controlling factors of movable fluids, and controlling factors of displacing efficiency in tight sandstone reservoirs are discussed. The study demonstrates that (1) the mean pore volume and permeability are 4.4% and 0.068 mD, respectively. The reservoir pertains to tight sandstone, mainly intergranular pore and dissolution pore, and the intercalated materials are mainly chlorite and illite. (2) The characteristic of the NMR T_2 spectrum has bimodal characteristics and can be subdivided into two classes: left peak dominant and right peak dominant. The mean value of mobile fluid saturation was 17.9%. (3) According to the relative permeability curve pattern, it is divided into four categories, and the mean bound water saturation is 29.9%. The average irreducible oil saturation was 40.6%. The mean oil flooding efficiency was 40.2%. (4) The better the pore-throat relationship, the lower the T_2 cutoff, the stronger ability of the fluid migration ability, and the higher of a percentage of active fluid. The percentage of active fluid in a low-permeability reservoir is affected by the reservoir's physical property and pore structure.

1. Introduction

With the quick increase in gas and oil energy consumption, conventional oil and gas energy sources are gradually depleted, and exploration and development are also increasing from usual reservoirs to low-permeability storage layers and then to compact sandstone reservoirs [1–5]. Compact sandstone reservoirs, as unconventional reservoirs, have gradually changed into a vital target for increasing gas-oil reserves and production [6–10]. Tight sandstone reservoirs are characterized by variable reservoir space types, complex pore structures, and mainly micro- and nanoscale pore throats, resulting in relatively complex fluid occurrence characteristics. The quantity and occurrence characteristics of active fluid are important for the evaluation of pore tortuosity-connectivity and calculation of the available reserves. This serious conditions the accurate evaluation and efficient exploitation of such reservoirs [11–16].

Through the investigation of domestic and foreign literature, it is found that there are many methods to study the porosity texture of compact sandstone reservoirs; meanwhile, by mercury penetration experiment and NMR test, the multiscale pore-porous distribution in compact sandstone reservoirs can be better obtained [17–28]. In recent years, researches on movable fluids in compact sandstone reservoirs are mainly focused on the evaluation of the saturation of movable fluids [17], while few studies on their occurrence characteristics in pores [12–21]. NMR and centrifugal tests can be utilized to better explore the content and reserve of movable fluid in compact sandstone

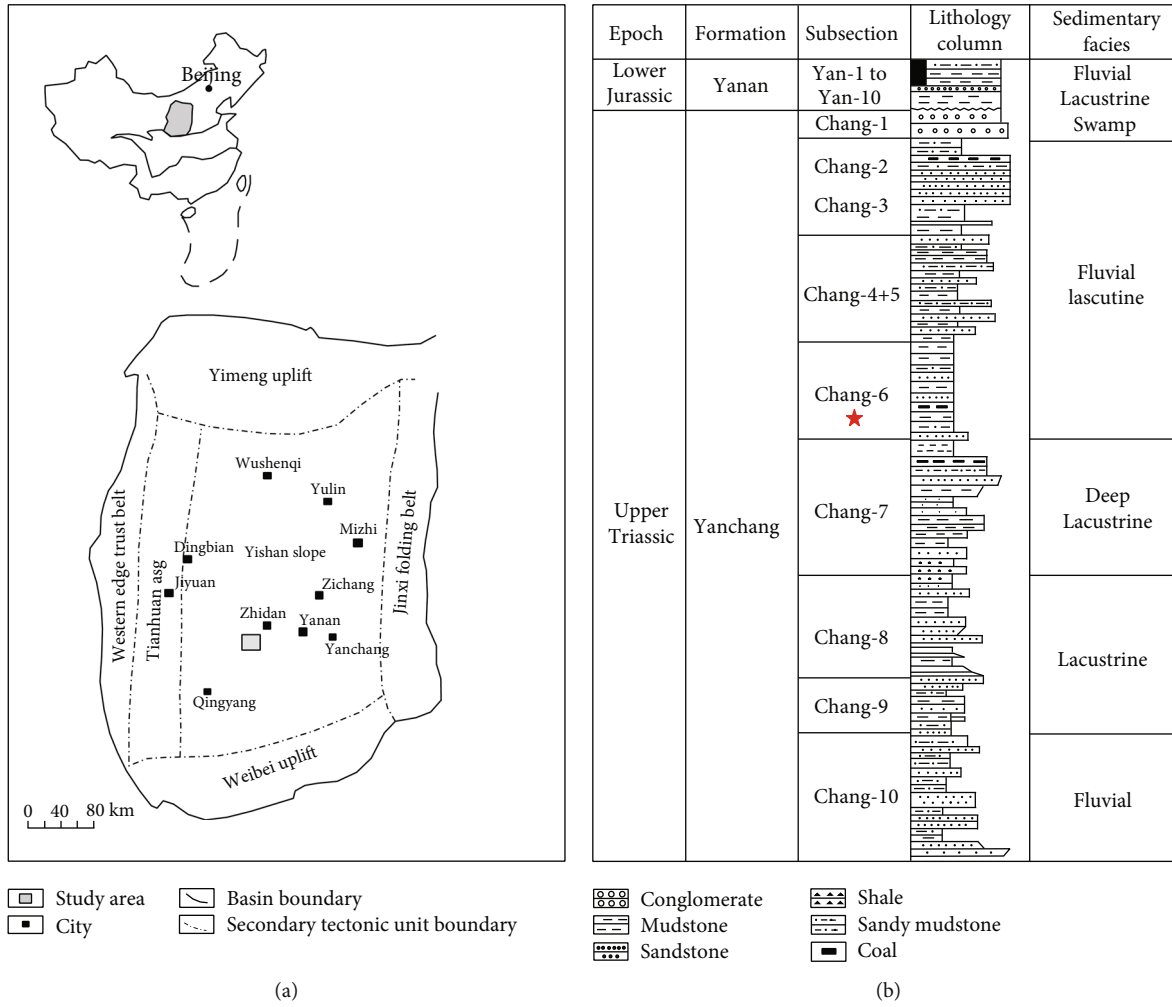

Figure 1: Overview of the research region: (a) location map of research region; (b) stratigraphic development feature in the study area.

reservoirs [22–32]. The study of compact sandstone reservoirs mainly focuses on pore structure and movable fluid. Compared with the study of these two aspects, the oil-water permeability experiment can reflect the flow situation under the coexistence of oil-water two phases; the obtained relative coefficient of permeability, bound water content, and irreducible oil content are more accessible to the real producing specificity [19, 32–35].

The exploration and development of the Baibao area have gone through three stages: a Jurassic reservoir, an upper reservoir of the Yanchang Formation, and a middle lower reservoir of the Yanchang group. Among them, the prospection and exploitation of the Chang 6 layer have become essential for the development of the Changqing Petroleum Enterprise. The production of the Chang 6_3 reservoir in the Baibao oilfield varies greatly, and the fluid distribution is complex. Therefore, the movable fluid of the Chang 6_3 reservoir in the Baibao oilfield is studied.

Therefore, this paper chose the Chang 6_3 reservoir as the research object in the Baibao oilfield of Ordos Basin based on a detailed study of reservoir geological characteristics using the instrumentation of rock slice, SEM, low-field NMR, and water-oil relative coefficient of permeability. The reservoir micropore structure, movable fluid distribution law, oil-water percolation, and oil flushing efficiency were studied, which provided a basis for comprehensive evaluation of the reservoir. Meanwhile, this research guides oil-gas investigation and exploitation in compact sandstone reservoirs.

2. Geology Setting

The Erdos Basin belongs to a Mesozoic-Cenozoic basin, distributed in five prefectures, with a total acreage of 25×10^4 km^2. Baibao is located in Wuqi prefecture, Shaanxi Province, and Huachi prefecture, Gansu Province, and is subordinate to the loess plateau landform (Figure 1(a)). Lie in the south of Yishan clivus, with gentle west-dip monoclinic, is the dip angle of which is less than one degree. The nose-shaped uplift formed by differential compaction is locally developed, and its axis is near the east-west or northeast [6–8]. The stratum from top to bottom in this area includes Quaternary, Tertiary, Lower Cretaceous (Zhidan Formation), Jurassic (Anding, Zhiluo, Yan'an, and Fuxian

Formations), and Triassic Yanchang Formation (Figure 1(b)). The main oil-bearing stratum is the Triassic Yanchang Formation, which is further divided into 10 oil formations. The main oil-bearing layers are Chang 8, Chang 6, Chang 4+5, etc., among which Chang 6 reservoir is a major oil-producing stratum of Baibao area of Changqing oilfield, and its sedimentary environment is an inland lacustrine delta sedimentary environment dominated by clastic rocks (Figure 1(b)) [15, 19, 31, 32]. The data of developed blocks show that the sand bodies in this area are widely distributed, the thickness of oil reservoirs is large, there is a strong reservoir heterogeneity and poor physical properties, the oil level is different, the horizontal change is fast, the oil production is low, the oil output decreases quickly after the oil output is put into operation, and the influencing factors of the production are complex. Compared with other developed dense reservoirs in the Ordos Basin, they have more compact lithology and finer pore throats. Feldspar sandstone and lithic feldspar sandstone are the main clay minerals in the reservoir, and rock bump constituents are mainly feldspar and quartz. The study of the reservoir and active fluid features has an important meaning for sustainable exploitation in the oilfield.

3. Methods

A series of analytical tests was performed on a 6_3-stage plug sample (diameter 2.5 cm and length 3 cm) drilled from coring wells in the study area. These test analyses mainly include conventional porosity-permeability measurement, casting slice identification, back-scatter electron microscope test, oil-water phase permeability test, and low-field NMR test.

The measurement instrument is the CM-300, porosity measurement is the volume method, and permeability is the measurement of air permeability, mainly to evaluate the accumulated ability and seepage characteristic; the test criterion is SY/T5336-2006.

3.1. Casting Thin Section. The rock mineral composition and pore configuration characteristics of the reservoir can be observed by casting thin slices. First, the core samples are ground to 0.03 mm and then fixed on the slide, and the rock pores are filled with red or blue resin. The pore space class and sizes of the reservoir are studied under the microscope, and the distribution and combination features of each class of pores are analyzed.

3.2. Scanning Electron Microscope. To investigate the composition of clay minerals in the rock and its distribution characteristics in pores, 20 blocks were elected for SEM analysis. Firstly, the fresh section of the specimen was plated with gold, and then, the experiment was carried out by a scanning electron microscope (JSM-5500LV) and an X-ray energy spectrometer (QUANTAX400) according to SY/T5162-2014 standard. Analyze the distribution characteristics of different types of clay minerals.

3.3. Nuclear Magnetic Resonance. The relaxation characteristics of low-field NMR can be applied to calculate the reservoir porosity, permeability, and content of bound fluid and active fluid and study the characteristics of pore texture of the reservoir strata. The detailed experimental process is as follows: the diameter of the plunger sample is 25 mm, and a length of 40 mm is drilled from the core. Wash the sample with oil and salt, and measure the permeability of the standard core after drying. Use a vacuum pump to vacuum the core sample, and then saturate the core sample with formation water. T_2 spectra of saturated formation water and centrifuged cores are measured to obtain the T_2 cutoff value and movable fluid characteristics. The equipment is Niumay mini-NMR, with an echo interval of 0.1 ms, waiting time of 2 s, temperature of 25°C, field strength of 0.5 T, scanning times of 128 times, and echo times of 10,000 times.

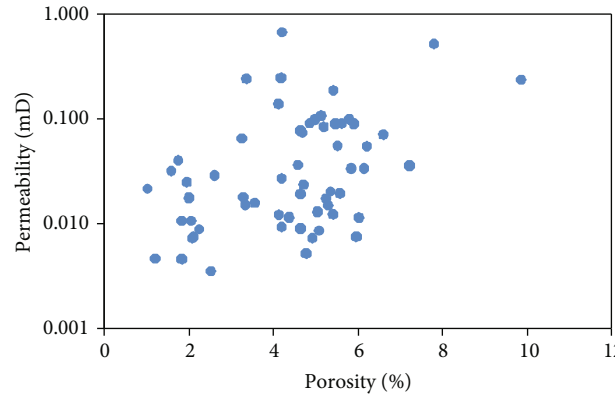

Figure 2: Porosity-permeability cross plot.

3.4. Relative Permeability Experiment. The permeability of the oil-water phase is measured by the unsteady-state method and tested according to the industry standard SY/T5345-2007. Micropumps select 100DX high-accuracy and high-pressure volumetric pumps. Firstly, the sample is vacuumed and dried, and then, the porosity and permeability are measured to calculate the efficient pore cubage. The plunger sample is first vacuumed and then saturated with the original formation water, and the salinity is 60,000 mg/L. Load the core into the core clamper and connect it to the test system. When the temperature rises to 65°C, the simulated oil (viscosity 51.6 MPa·s) is infused into the samples, measuring the volume of discharged water and calculating water saturation. Water displacement is carried out with a fixed rate of flow of 0.05 mL/min. During the displacement process, measure the content of oil and water at the outlet until no oil flows out at the outlet, end the experiment, and calculate the remaining oil saturation in the core sample.

4. Results

4.1. Characteristics of Reservoir Physical Property. Figure 2 shows the analysis results of porosity and permeability of about 60 cores, with the porosity distribution from 1 to 9.9%, with a mean of 4.4%. The permeability distribution is 0.004-0.677 mD, with a mean of 0.068 mD. The reservoir is mainly depicted by small porosity and extremely poor permeability. The permeability increases with the increase of

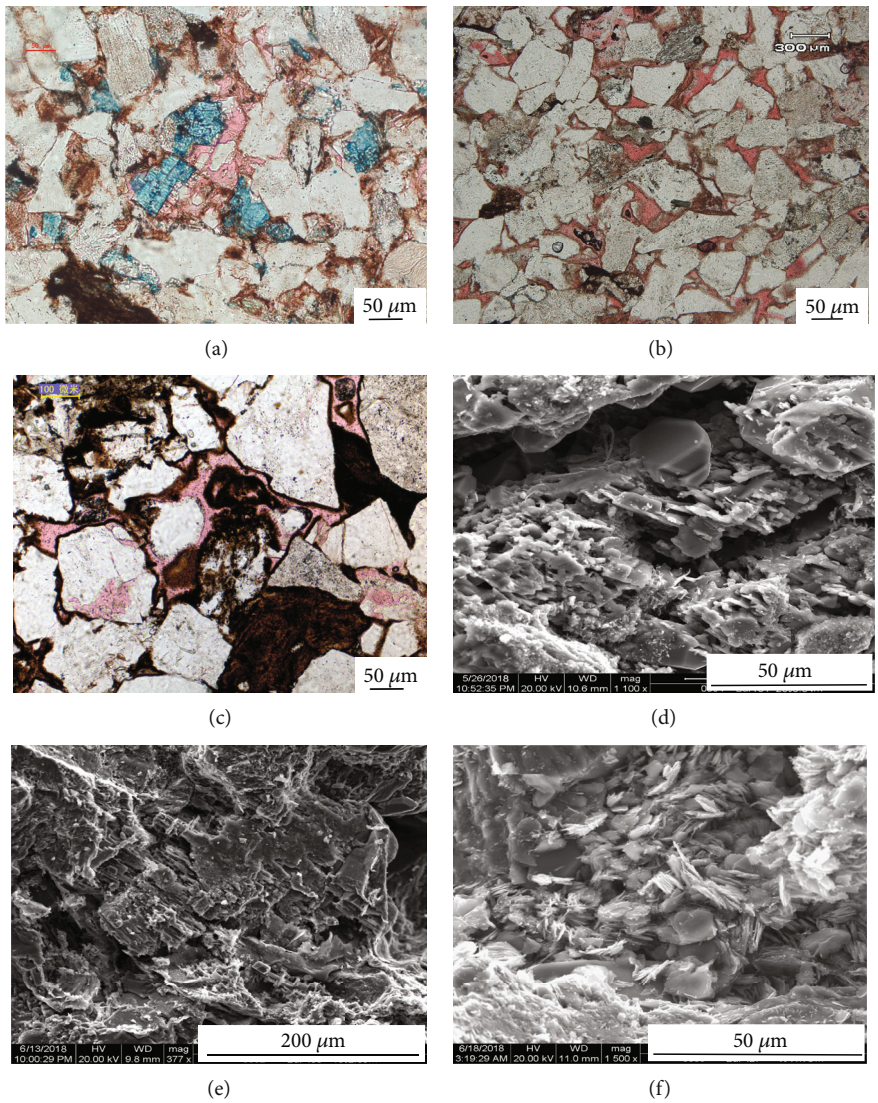

Figure 3: Pore structure characteristic diagram: (a) Bai 409,2153.6 m, dissolution hole; (b) Bai 413,2181.4 m, intergranular pores and dissolution pores; (c) Bai 406,1979.81 m, intergranular pore; (d) Bai 131,2056.3 m, a small amount of feldspar is dissolved to produce soluble pores; (e) Bai 406,1982.6 m, particle dissolution residual form; (f) Bai 427,1941.8 m, a small amount of filled kaolinite will petrochemical in some pores.

porosity, but the correlation coefficient is low. Under the same porosity, permeability varies greatly, and the pore structure is complex (Figure 2).

4.2. Feature of Reservoir Pore Structure. According to the observation of the rock thin section, the red and blue filling parts are pore spaces. In Figure 3(a), the compaction in a reservoir is strong, and the rock granules are mainly in linear contact, mainly in dissolution pores and mainly in the dissolution of feldspar particles. In Figure 3(b), the reservoir is mainly characterized by line contact and mainly contains residual intergranular pores. Figure 3(c) is mainly characterized by residual intergranular pores, and the surrounding particles are wrapped by chlorite film. Figures 3(d) and 3(e) show the dissolution of feldspar particles under SEM. Figure 3(f) shows intergranular pores filled with kaolinite

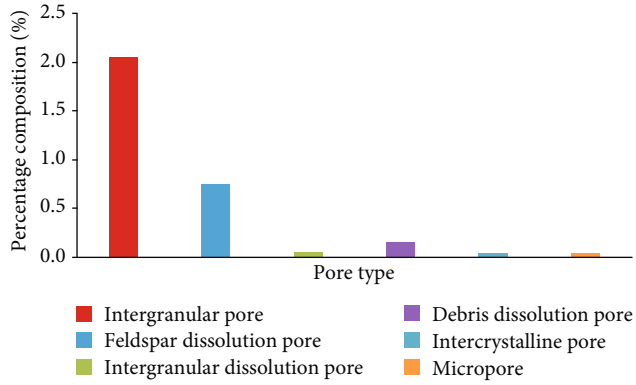

Figure 4: Statistical histogram of pore types.

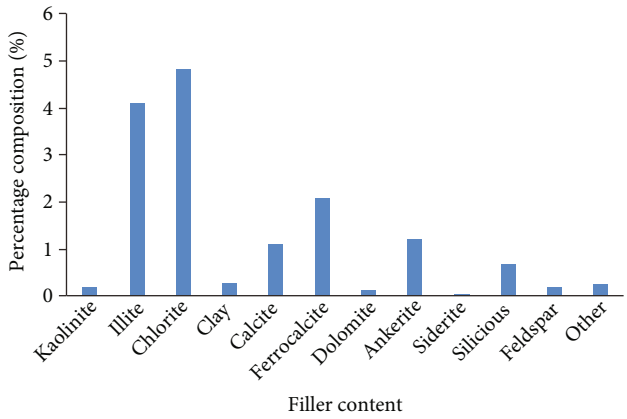

Figure 5: Statistical histogram of filler content.

and calcite. The average face rate of the reservoir is 3.12%, mainly intergranular pores and dissolution pores (Figure 4).

The content of reservoir interstitials in the research area is 15.15%, and the contents of various interstitials are different, mainly chlorite and illite, which are 4.1% and 4.8%, respectively. A small amount of carbonate mineral components was developed, with 1.1% of calcite, 2.1% of iron interpretation, and 1.2% of iron dolomite (Figure 5). The high content of reservoir interstitials fills voids and throats and affects pore structure and physical properties.

4.3. Nuclear Magnetic Resonance Characteristics of the Reservoir. The attenuation of the NMR signal is the superposition of the decay of the fluid signal in the pore, corresponding to the long attenuation time of the big aperture and the short attenuation time of the small aperture. Select 15 samples for NMR experiments. Figure 6(a) shows the T_2 spectrum of saturated underwater nuclear magnetic resonance. The T_2 spectrum was distributed between 0.1 and 100 ms, which could be classified as bimodal form and unimodal form according to the morphology of the T_2 spectrum. The unimodal type mainly developed a small pore throat, and the spectral peak was concentrated between 0.1 and 1 ms with a peak value of 0.5 ms. According to T_2 spectral peak characteristics, the bimodal is further divided into the left apex bigger than the right and the right apex bigger than the left. There are two types of porous throat in the reservoir: small pore throats are mainly distributed in 0.1~1 ms with a peak value of 0.5 ms, and large pore throats are distributed in 2~100 ms with a peak value of 10 ms. Figure 6(b) shows the T_2 spectrum of immobile water. Compared with the T_2 spectrum distribution in the saturated original formation water state and immobile water state, the site of the spectral peak did not change, but the peak height became smaller, especially the right peak changed greatly, reflecting the movable fluids mainly occurring in macropore throat.

A line parallel to the x-axis is drawn from the endpoint value of the accumulated curve of the centrifuged T_2 spectrum, and it has an intersection with the mass curve of the impregnated water state, and the T_2 corresponding to the crossover point value is defined as the T_2 cutoff value (Figures 7(a), 7(c), and 7(e)). T_2 cutoff values ranged from 4.2 ms to 150 ms, with an average of 34.2 ms. The T_2 cutoff value of the reservoir is not fixed, and the size is associated with the pore texture. The higher the ratio of large pores and throats, the smaller the T_2 cutoff. The T_2 cutoff divides the T_2 spectrum into two parts for water-saturated states. Those above the T_2 cutoff are movable fluids, and those below the T_2 cutoff are bound fluids. The movable fluid saturation ranges from 3.1% to 46.6%, and the average value is 17.9%. The porosity of movable fluid ranges from 0.1% to 5.5%, and the average value is 1.6%. The geometric mean value of T_2 ranged from 0.615 ms to 2.711 ms, and the mean value was 1.607 (Table 1). According to the position of the separation point on the pore size distribution curve after water saturation condition and centrifugation, the corresponding least radius of pore active fluid was determined to be 4 nm (Figures 7(b), 7(d), and 7(f)).

By comparing the T_2 spectra of impregnated and bound water states, the active fluid is mainly distributed in bigger pore throat, and the pore-throat size is concentrated in 0.001 μm~2 μm. In Figure 7(a), the porosity of No. 30 is 4.9%, the permeability of No. 30 is 0.0004 mD, and the porous-throat size ranges from 0.001 μm to 1 μm. The porous throat is mainly small and less macropore development, and the mobile fluid saturation is 7.6% (Figure 7(b)). In Figure 7(c), the porosity of sample No. 9 is 7.6%, the permeability of No. 9 is 0.0239 mD, and the porous-throat size ranges from 0.001 μm to 1 μm. The left apex is slightly bigger than the right apex. Both small and large porous throat are developed, and the saturation of active fluid of sample 30# is 21% (Figure 7(d)). In Figure 7(e), the porosity of sample No. 47 is 10.9%, the permeability is 0.191 mD, the radius of pore size ranges from 0.001 μm to 1 μm, the right apex is slightly bigger than the left apex, the macropore throat is developed than the small hole, and the mobile fluid saturation is 27.7% (Figure 7(f)).

The distribution of pore throat radius in the reservoir is between 0.001 and 2 μm. The pore throat of nanopore is smaller than 0.1 μm; the pore throat of micropores is between 0.1 and 2.5 μm; the pore throat of mesoporous is between 0.5 and 0.5 μm; the pore throat of macroholes is between 2.5 and 10 μm; and the pore throat of giant hole is larger than 10 μm. The pore volume of a nanopore in the study area is 1.74-6.51%, the average value is 4.58%, and the proportion is 55.8%-90.3%, with a mean of 71.3%. The pore volume of micropores is 0.08-3.74%, the average value is 1.52%, and the proportion is between 4 and 33.2%, with an average value of 18.7%. The pore volume of mesoporous pores was 0.04-2.02%, the average value is 0.64%, and the proportion was 1-25.8%, with an average value of 8.5% (Figures 8(a) and 8(b)). Macroholes and giant holes are relatively small. The reservoir is dominated by nanopores, controlling 48% of the movable fluid, while micropores and mesopores control 50.6% of the active fluid, and the active fluid is major affected by macropores and throats. The proportion of the movable fluid in nanopores in the research area is high, which is mainly because of the high proportion of nanopore volume (Figure 8(c)).

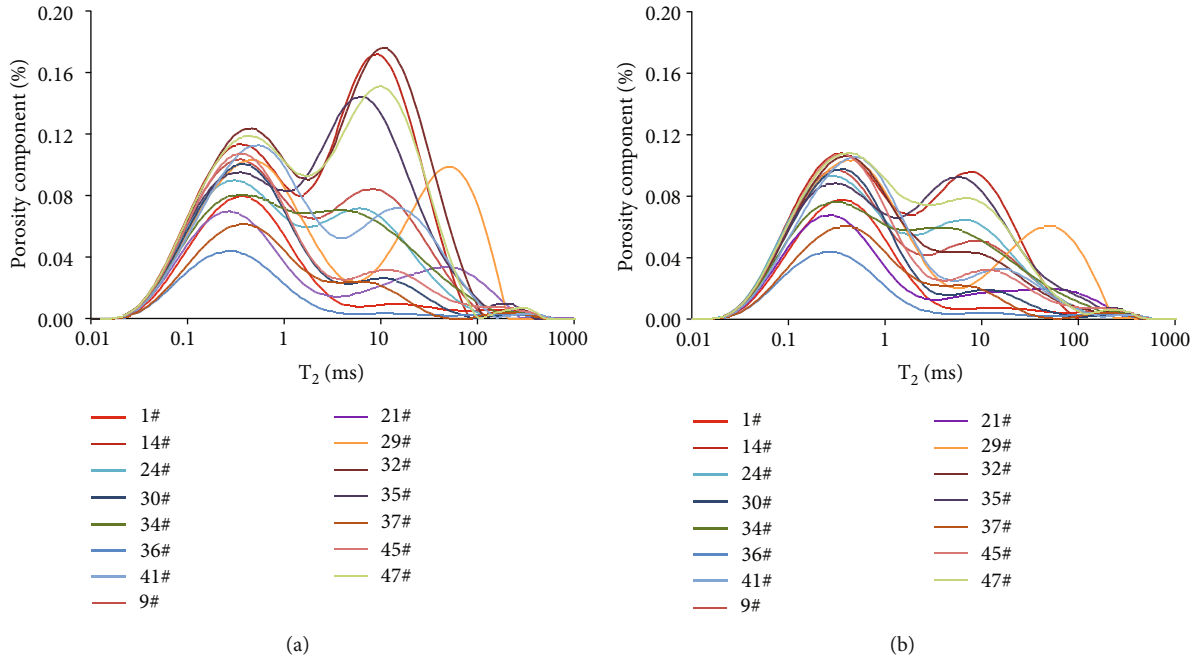

Figure 6: Nuclear magnetic resonance T_2 spectrum: (a) T_2 spectrum of saturated water state; (b) postcentrifugal T_2 spectrum.

4.4. Reservoir Relative Permeability Results. Oil-water phase permeability experiment can truly reflect how the oil phase migrates in the reservoir when there are both oil and water fluids in reservoir pores. Irreducible oil saturation and immobile water saturation obtained by the oil-water relative permeability experiment may be closer to the real production data, and the water breakthrough characteristics in the production process are judged by the feature of the relative infiltration rate curve.

Statistical results of the relative infiltration rate experiment of 8 samples show that the bound water saturation ranges from 22.3% to 38%, and the mean value is 29.9%. Irreducible oil saturation ranged from 37% to 44.6%, and the mean value is 40.6%. The oil saturation of isotonic points is distributed in 39.9%~ 59.5%, and the mean value is 49.6%. The reservoir is mainly hydrophilic or neutral wetting. The relative permeability of isotonic points ranged from 0.068 mD to 0.158 mD, with an average of 0.124 mD. The width of the oil-water two-phase band ranges from 21.1% to 37.2%, with a mean value of 29.5%. The oil displacement efficiency ranges from 34.1% to 48.7%, with an average of 40.2 (Table 2).

Based on the curve of oil-phase and liquid-phase relative seepage, it is divided into four classes. In Figure 9(a), the porosity of No. 29 is 3.24%, the permeability is 0.065 mD, the bound water saturation of No. 29 is 31.2%, and the irreducible oil saturation of No. 29 is 44.6%. With water saturation going up, oil-phase permeability declines stably, and the water percolation capacity grows tardy in the beginning and later grows faster. The seepage capacity of the oil-water intersection point is high. In Figure 9(b), the porosity of No. 35 is 4.1%, the permeability of No. 35 is 0.139 mD, the bound water saturation of No. 35 is 38%, and the irreducible oil saturation of No. 35 is 40.8%. With water saturation going up, the oil phase relative permeability begins to decrease stably, then the decrease rate becomes slow, and the water phase begins to grow rapidly; then, the growth rate becomes slow. In Figure 9(c), the porosity of No. 47 is 3.35%, the permeability of No. 47 is 0.242 mD, the bound water saturation of No. 47 is 35.7%, and the irreducible oil saturation of No. 47 is 37.4%. Following water saturation going up, the initial decrease rate of the oil phase is fast, and then, the decrease rate is gradually slow. Figure 9(d) shows that the porosity of No. 49 is 5.61%, the permeability of No. 49 is 0.09 mD, the binding water content of No. 49 is 25.8%, and the remnant oil saturation is 37.1%. Following water saturation going up, the oil phase initially decreases faster and then decreases slowly, and the water phase begins to grow slowly, then grows faster, and then grows slowly. The better the reservoir seepage capacity, the wider of the width of the copermeability zone, the smaller the residual oil saturation, and the bigger the oil displacement efficiency.

Figure 10(a) shows the variation feature of oil flooding efficiency of the four samples with the raise of injected water multiples. No. 49 has good porosity-permeability and the fastest growth of oil flooding efficiency. Water injection times reach 0.7, and the oil flooding efficiency reaches the peak and then remains unchanged as the raise of water injection. For the 35# sample, the oil flooding efficiency reaches the peak when the injection water multiple reaches 0.95 times, and the oil flooding efficiency slowly rises with the continuous water injection. The oil flooding efficiency of No. 29 reaches the peak when water injection times reach 1.7 and changes little with the continued water injection. Combined with Figure 8(a), for low seepage capacity reservoirs, the larger the permeability, the larger the percentage contents of large pore throats,

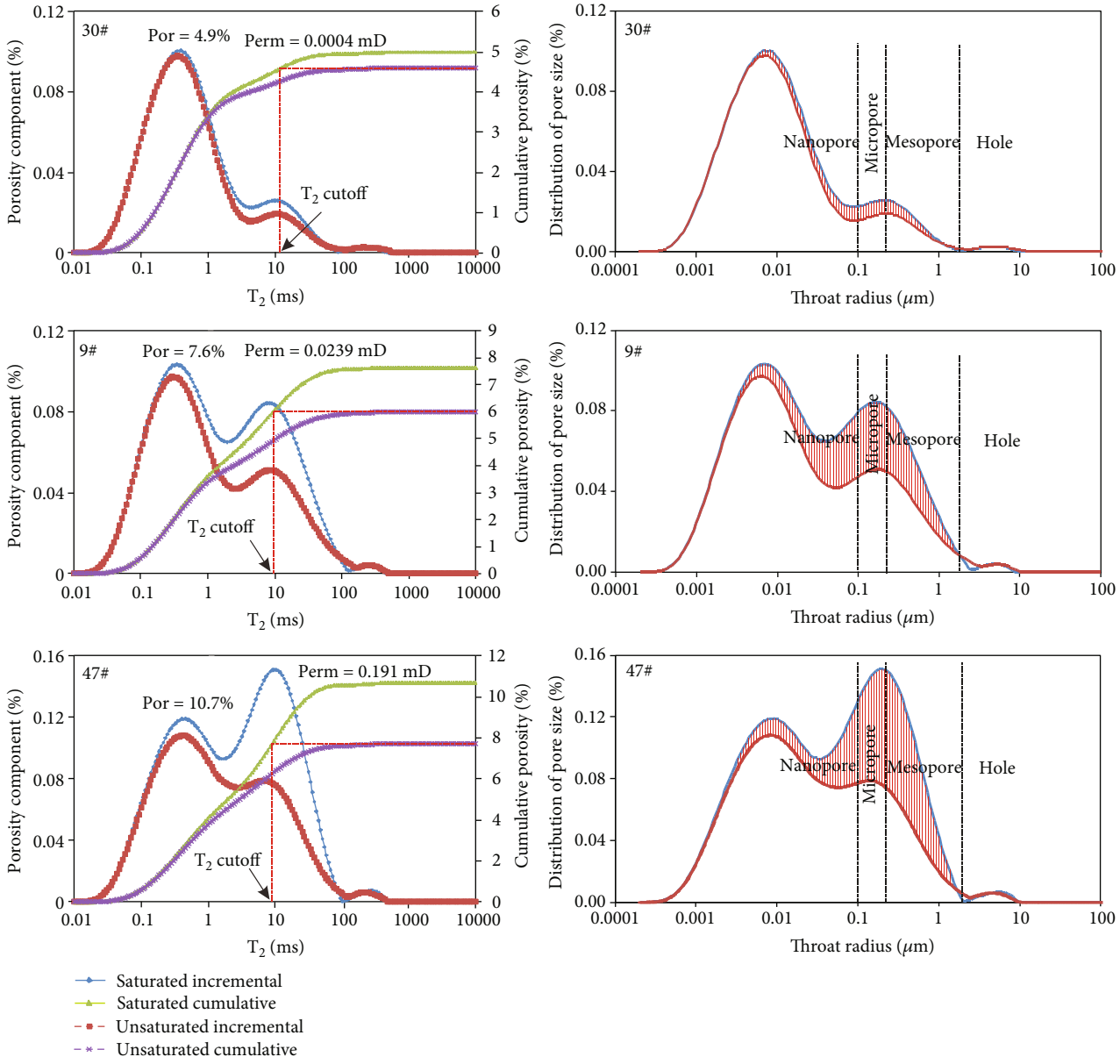

Figure 7: NMR T_2 spectrum and pore-throat distribution diagram.

the bigger the recovery efficiency during the injection of water, and the less injected water consumption to achieve the same recovery degree. The 47# sample has a double peak structure, the right peak is bigger than the left, and the injected water first enters into the bigger pore volume. Along with the raise during the water injection, the water gradually injects into the small pore throat, and the oil flooding efficiency gradually rises. As the water injection volume reaches 3 times, the flooding capacity of oil gradually gets stable; moreover, the oil flooding efficiency is the highest.

Figure 10(b) shows the variation characteristics between water injection multiple and water production rates in about four samples. The water production rate curve of sample 29# increases stably with the raise of the volume of water infused, and the water production rate of the other three samples all shows multistage characteristics. In the early water injection, the 49# sample has a relatively long stable production, while the water content of the other three samples rises rapidly. As the raise of the water infusion multiple, when the water infusion multiple is 0.18, the water content of the 47# sample quickly reaches the first inflection point of 62%; when the water injection multiple is 0.20, the water content of the 35# sample reaches the first inflection point 73%; when the water injection multiple is 0.23, the water content of 49# reaches the first inflection point 86%. The moisture content of the 29# sample slowly increases with the raise of water injection times. The stable production time is relatively short. It can be seen from Figure 6 that 29# is a double peak type with the same left and right peaks, and the reservoir permeability

Table 1: NMR test results.

No.	Nuclear magnetic porosity (%)	Permeability (10^{-3} μm^2)	Movable fluid porosity (%)	T_2 cutoff (ms)	T_2 geometric mean (ms)	Movable fluid saturation (%)
1	3.7	/	0.2	41.5	0.6	4.7
9	7.6	0.024	1.6	9.7	1.5	21.0
14	10.7	0.147	2.8	10.4	2.3	25.0
21	4.2	0.001	0.5	47.7	1.4	12.2
24	6.5	/	0.1	95.0	1.3	0.9
29	7.8	0.009	1.1	58.7	2.7	13.3
30	5.0	0.001	0.4	12.8	0.7	7.6
32	11.7	1.412	5.5	4.2	2.6	46.6
34	6.5	0.002	0.7	22.2	1.5	10.0
35	9.6	0.073	2.2	10.4	2.2	22.5
36	1.9	/	0.0	150.0	0.5	1.1
37	3.3	/	0.1	23.8	0.8	3.1
41	7.6	0.036	1.9	8.4	1.6	24.9
45	5.6	0.003	0.8	9.7	0.8	14.2
47	10.7	0.191	3.0	9.0	2.2	27.7

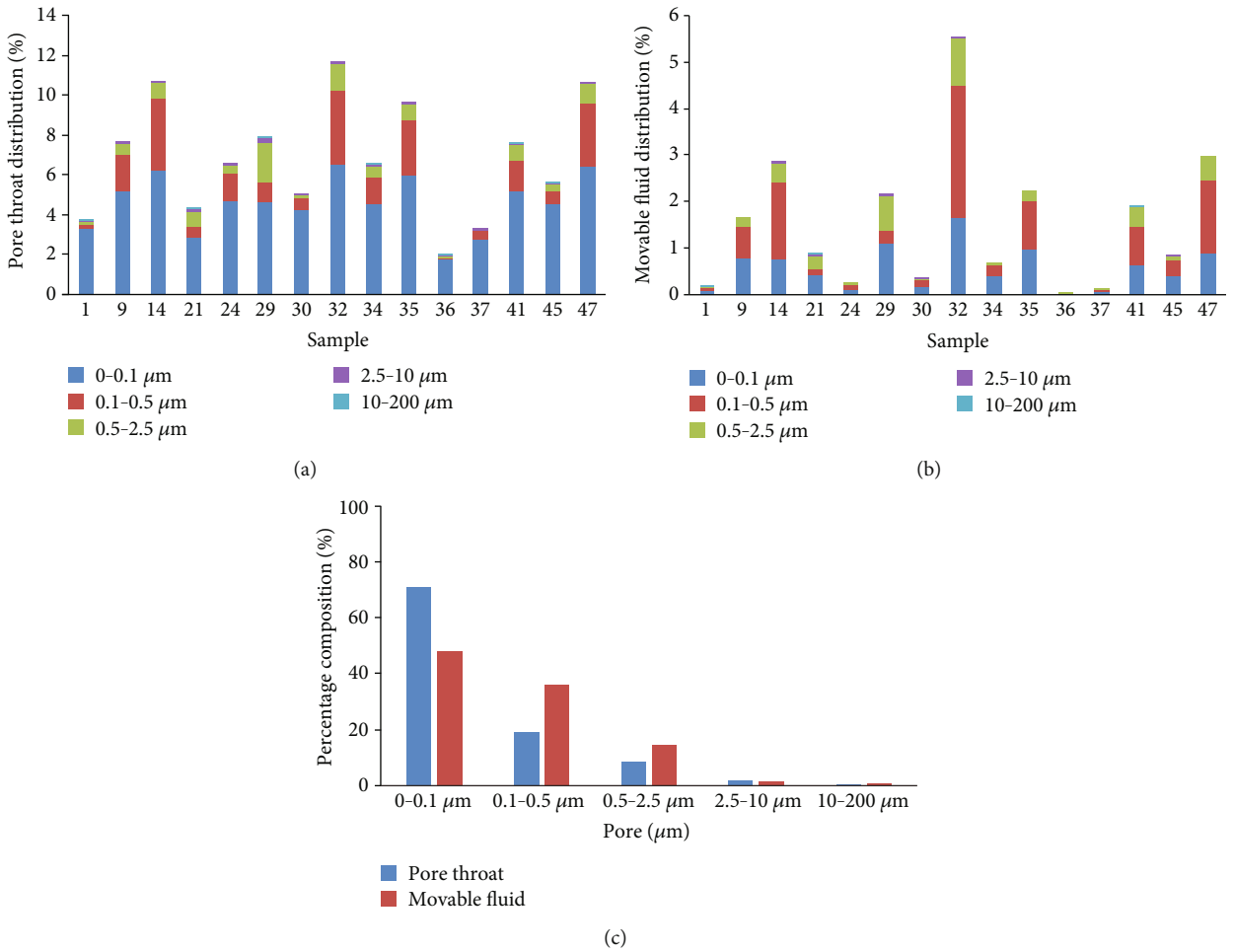

Figure 8: Statistical histogram of the reservoir: (a) percentage content of porous throat in different sizes in different samples; (b) percentage content of active fluid governed by various pore throats in different specimens; (c) proportion of active fluid governed by various pore throats.

Table 2: Experimental results of relative permeability.

No.	Porosity (%)	Permeability ($\times 10^{-3}$ μm^2)	Irreducible water saturation (%)	Isotonic point water saturation (%)	Oil-water relative permeability (mD)	Irreducible oil saturation (%)	Two-phase infiltration width	Oil displacement efficiency (%)
9	4.2	0.677	22.3	49.6	0.152	43.4	34.3	44.1
29	3.2	0.065	31.2	49.6	0.158	44.6	24.2	35.2
30	2	0.018	22.4	49.6	0.151	43.4	34.2	44.1
33	10.4	0.31	25.8	59.5	0.078	37	37.2	44.1
34	1.6	0.032	38.0	51.2	0.114	40.9	21.1	34.1
35	4.1	0.139	38.0	50.6	0.124	40.8	21.1	34.1
47	3.4	0.242	35.6	46.7	0.068	37.4	27.0	48.7
49	11.6	0.262	25.8	39.9	0.143	37.1	37.1	37.2

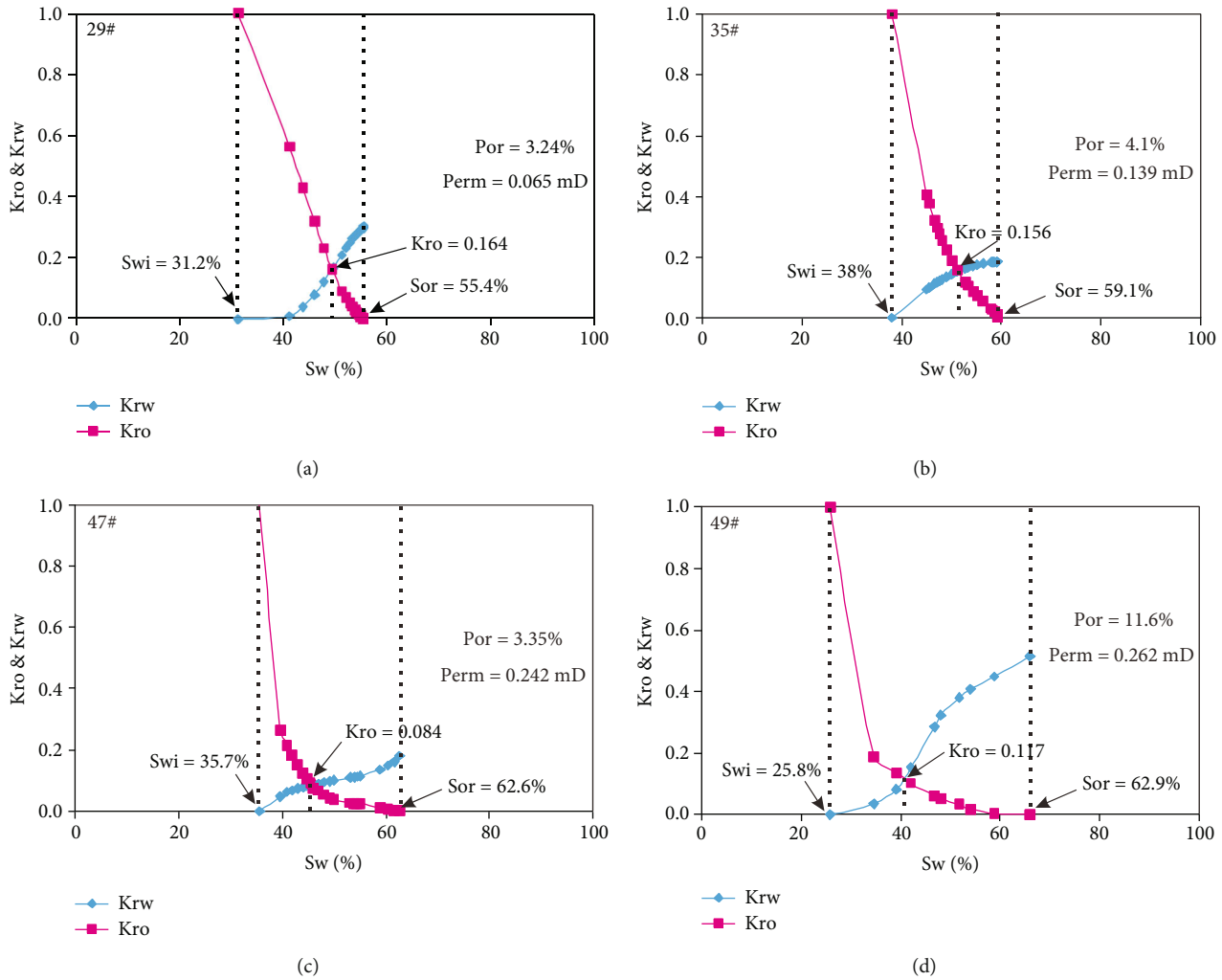

Figure 9: Characteristics of different kinds of oil-water permeability curve.

is poor, so the injected water is difficult to burst and water is seen slowly. The right peak of both 35# and 47# samples is bigger than that of the left peak, the reservoir permeability is better, and the water appears faster. The micropore texture in a low seepage capacity reservoir has a strong control effect on oil flooding efficiency and water content.

5. Discussion

5.1. Controlling Factors of T_2 Cutoff Value. The T_2 cutoff of the reservoir is very important for calculating permeability and movable fluid by NMR logging. Based on the test results of NMR, the T_2 cutoff value of the reservoir is not

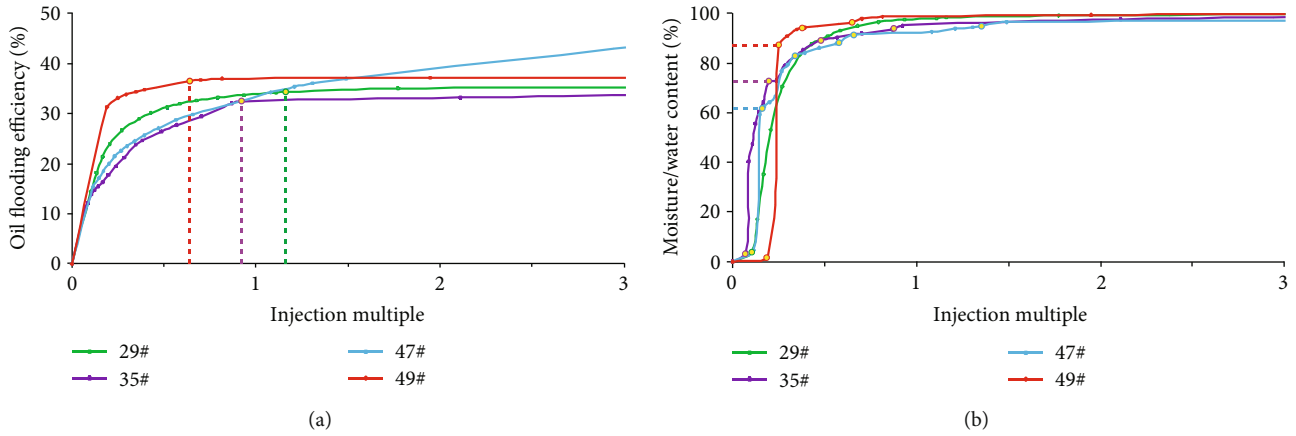

Figure 10: (a) Relationship between water injection multiple. (b) Oil flooding efficiency and water content.

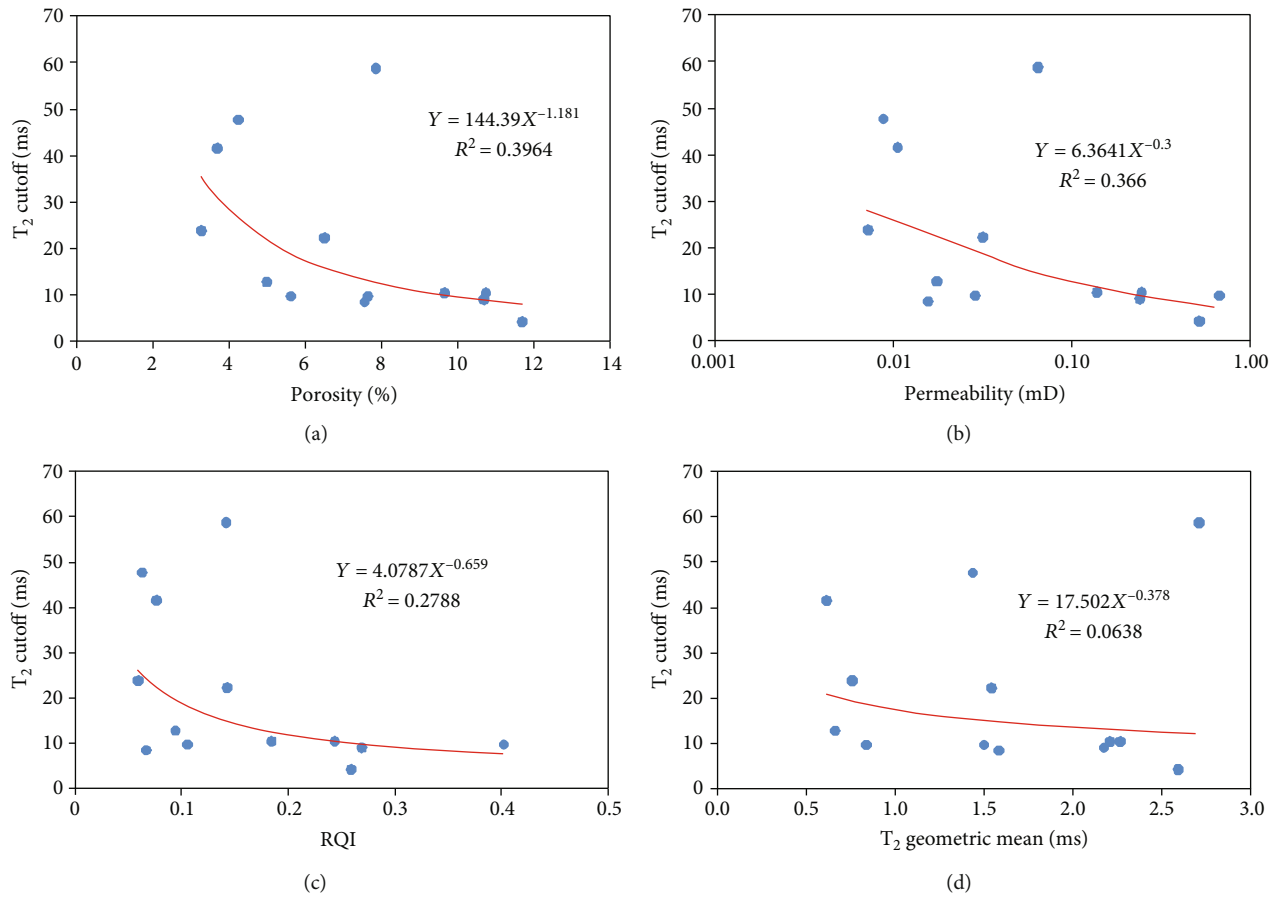

Figure 11: Influencing factors of T_2 cutoff value: (a) cross plot with T_2 cutoff value of porosity; (b) cross plot with T_2 cutoff value of permeability; (c) cross plot with T_2 cutoff value of RQI; (d) cross plot with T_2 cutoff value of T_2 geometric mean.

a definite value and is controlled by the pore structure of the reservoir. The variation characteristics between T_2 cutoff and porosity, permeability, reservoir quality index, and T_2 geometric mean were statistically analyzed, and the influencing factors of T_2 cutoff value were studied. T_2 cutoff and porosity have a negative correlation; that is, the higher the porosity, the smaller the T_2 cutoff (Figure 11(a)). T_2 cutoff and permeability have a negative correlation; as the permeability increases, the T_2 cutoff value decreases (Figure 11(b)). The reservoir quality index was minus connection with the T_2 cutoff, and the better pore structure, the smaller the T_2 cutoff (Figure 11(c)). T_2 cutoff and geometric mean of T2 spectral have a negative correlation; with the decrease in geometric mean of T_2

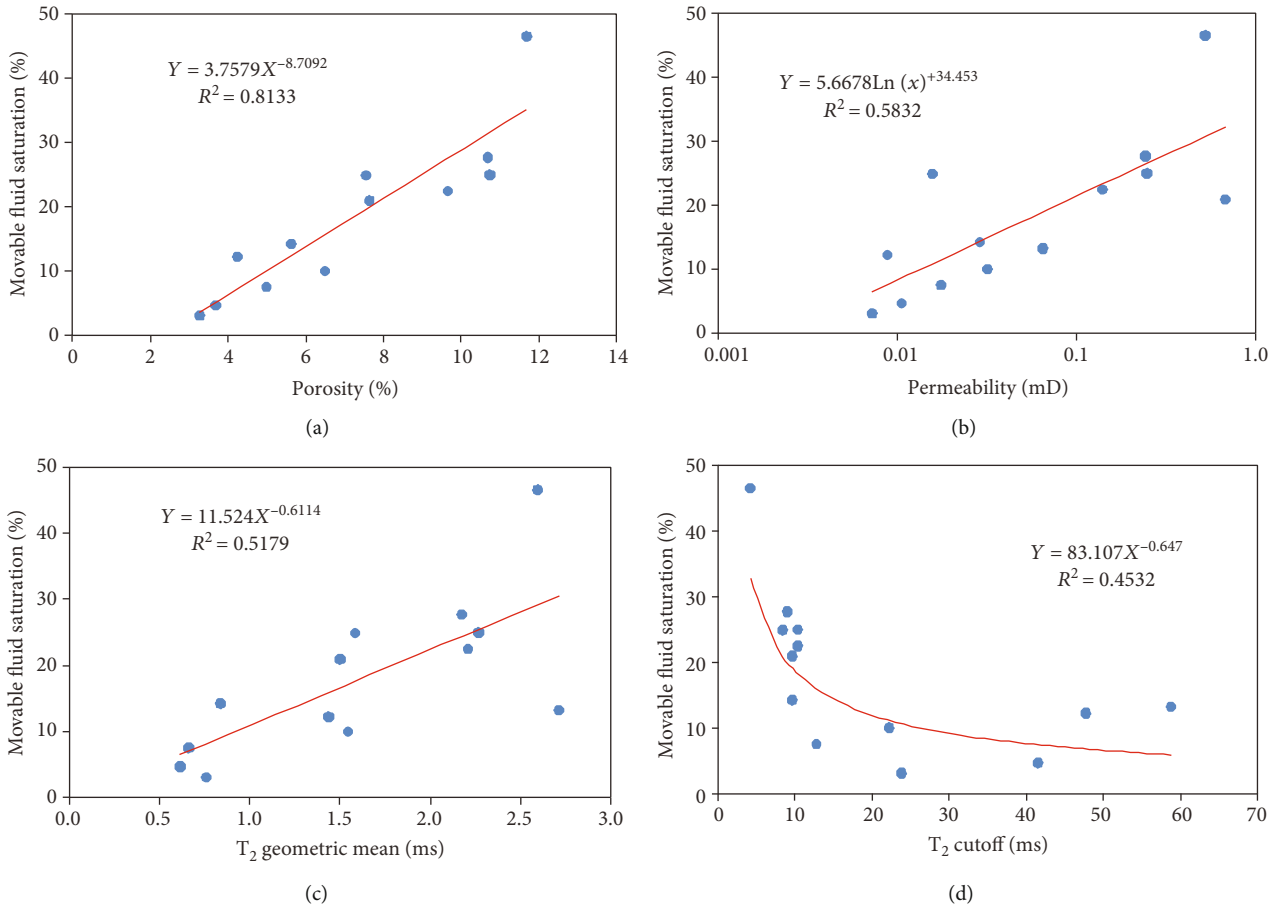

Figure 12: Analysis of influencing factors of movable fluid: (a) intersection diagram of porosity and active fluid percentage contents; (b) intersection diagram of permeability and active fluid percentage contents; (c) intersection diagram of T_2 geometric and movable fluid saturation; (d) intersection diagram of T_2 cutoff and movable fluid saturation.

spectral, the T_2 cutoff value also decreases (Figure 11(d)). If the pore texture of the reservoir is better, the lower the T_2 cutoff, the better the fluid migration ability, and possibly the bigger the fluid saturation. The calculation model of the variable T_2 cutoff value was established according to the macroscopic and microscopic parameters of reservoirs.

5.2. Controlling Factors of Movable Fluid. Movable fluid in reservoir has a very important meaning in reservoir development. Through analyzing the variation characteristic between porosity, permeability, T_2 geometric mean, T_2 cutoff value, and active fluid saturation, the controlling effect of active fluid saturation is analyzed. A positive connection is active fluid saturation and porosity. The larger the pore space, the lower the fluid migration resistance, and the higher the mobile fluid saturation (Figure 12(a)). There is a positive connection between active fluid saturation and permeability; that is, the better the seepage capacity of the reservoir, the higher the active fluid saturation (Figure 12(b)). There is a positive connection in active fluid saturation T_2 geometric mean. The higher the T_2 geometric mean is, the more percentage contents the macropore throat of the specimen, and the higher the active fluid saturation (Figure 12(c)). There is a negative connection in mobile fluid saturation and the T_2 cutoff. The lower the T_2 cutoff was, the bigger the percentage contents of the macropore throat were, and the higher the mobile fluid saturation was (Figure 12(d)). The active fluid percentage contents of a tight reservoir are controlled by the reservoir physical property and pore structure. The better the reservoir pore-throat connectivity, the higher the active fluid percentage contents.

5.3. Controlling Factors of Oil Flooding Efficiency. Low-permeability oil flooding efficiency plays a vital parameter in the economic recovery of the oil field. The relationship between porosity, permeability, reservoir quality index, T_2 cutoff value, T_2 geometric mean, movable fluid saturation, and oil flooding efficiency is analyzed, and the controlling effect on reservoir recovery degree is discussed. There is a weak positive correlation between oil flooding efficiency and porosity, and porosity has a weak control effect on oil flooding efficiency in compact reservoirs (Figure 13(a)). There is a weak positive correlation in oil flooding efficiency and permeability, and permeability has a certain control effect on oil flooding efficiency of compact reservoirs (Figure 13(b)). There is a positive connection in oil flooding ability and reservoir quality index. If the reservoir pore structure is better, the higher the oil flooding ability

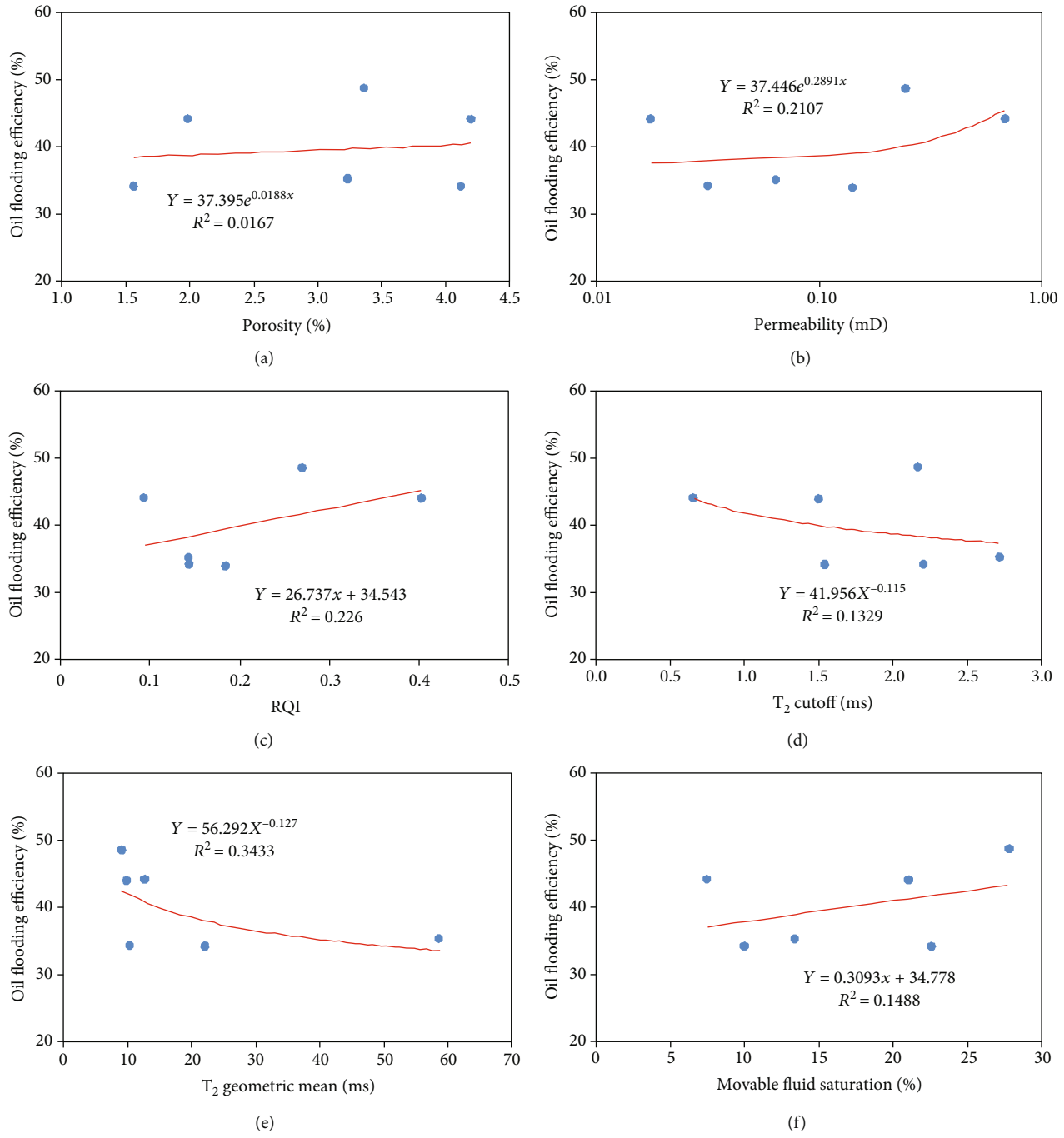

Figure 13: Analysis of influencing factors of oil flooding efficiency: (a) intersection diagram of porosity and oil flooding efficiency; (b) intersection diagram of permeability and oil flooding efficiency; (c) intersection diagram of RQI and oil flooding efficiency; (d) intersection diagram of T_2 cutoff and oil flooding efficiency; (e) intersection diagram of T_2 geometric and oil flooding efficiency; (f) intersection diagram of T_2 movable fluid saturation and oil flooding efficiency.

(Figure 13(c)). The T_2 cutoff value of the reservoir is minus connection with oil displacement efficiency. The bigger the T_2 cutoff value, the worse the development of a large porous throat, and the smaller the oil flooding ability (Figure 13(d)). Oil flooding efficiency has negatively correlated with the T_2 geometric mean value. The larger the geometric mean value of T_2, the more macropores are developed, and the bigger the oil flooding efficiency is (Figure 13(e)). There is a positive connection between oil flooding efficiency and movable fluid percentage contents. The larger the active fluid percentage contents, the better the pore space size and connectivity, and the bigger the oil flooding efficiency (Figure 13(f)). The displacement efficiency of oil in a tight reservoir is major influenced by pore structure and connected large pore throat.

6. Conclusion

(1) The mean value of porosity is 4.4%. The permeability is 0.068 mD. The reservoir is mainly characterized by micropores and extremely extralow permeability. The main pore types are intergranular pores and dissolution pores

(2) The NMR of reservoir specimens mainly developed bimodal type. The mean value of mobile fluid saturation was 17.9%. The active fluid controlled by nanopores reached 48%. The minimum aperture of the movable fluid is 4 nm

(3) The relative permeability curve is separated into four classes, and the average bound water saturation is 29.9%. The average irreducible oil saturation was 40.6%. The average width of the oil and water two-phase band is 29.5%. The mean oil flooding efficiency was 40.2%. The microscopic pore texture in extralow permeability storage layers has a strong control effect on oil flooding efficiency and water cut

(4) The active fluid percentage contents of low-permeability storage layers are controlled by reservoir physical property and pore structure. The better the storage layers' pore-throat connectivity, the higher the active fluid percentage contents. The final displacement efficiency is also germane to the pore system of the reservoir

Data Availability

The data applied to support the conclusions of this research are involved in the paper.

Conflicts of Interest

The authors proclaim that they have no benefit conflicts.

Acknowledgments

This paper was supported by the Scientific Research Program funded by the Shaanxi Provincial Education Department (Program No. 22JK0504) and Natural Science Basic Research Plan in Shaanxi Province of China (Program No. 2023JCQN0314).

References

[1] L. Chen, K. Liu, S. Jiang, H. Huang, J. Tan, and L. Zuo, "Effect of adsorbed phase density on the correction of methane excess adsorption to absolute adsorption in shale," *Chemical Engineering Journal*, vol. 420, article 127678, 2021.

[2] W. Ji, F. Hao, Y. Song, J. Tian, M. Meng, and H. Huang, "Organic geochemical and mineralogical characterization of the lower Silurian Longmaxi shale in the southeastern Chongqing area of China: implications for organic matter accumulation," *International Journal of Coal Geology*, vol. 220, article 103412, 2020.

[3] H. Huang, R. Li, Z. Lyu et al., "Comparative study of methane adsorption of Middle-Upper Ordovician marine shales in the western Ordos basin, NW China: insights into impacts of moisture on thermodynamics and kinetics of adsorption," *Chemical Engineering Journal*, vol. 446, article 137411, 2022.

[4] B. Zhao, R. Li, X. Qin et al., "Geochemical characteristics and mechanism of organic matter accumulation of marine-continental transitional shale of the Lower Permian Shanxi formation, southeastern Ordos basin, North China," *Journal of Petroleum Science and Engineering*, vol. 205, article 108815, 2021.

[5] K. Zhang, Y. Song, C. Jia et al., "Formation mechanism of the sealing capacity of the roof and floor strata of marine organic-rich shale and shale itself, and its influence on the characteristics of shale gas and organic matter pore development," *Marine and Petroleum Geology*, vol. 140, article 105647, 2022.

[6] R. Nie, J. Zhou, Z. Chen, J. Liu, and Yi. Pan, "Pore structure and movable fluid characteristics of tight sandstone reservoirs in the Upper Shihezi formation in Hangjinqi area, Ordos basin," *Bulletin of Geological Science and Technology*, vol. 5, no. 3, pp. 25–34, 2022.

[7] Z. Lu, C. Liu, Q. Zang et al., "Application of high pressure mercury injection and nuclear magnetic resonance in analysis of the pore structure of dense sandstone; a case study of the Heshui area, Ordos basin," *Bulletin of Geological Science and Technology*, vol. 41, no. 3, pp. 300–310, 2022.

[8] W. Ji, Y. Song, Z. Jiang, X. Wang, Y. Bai, and J. Xing, "Geological controls and estimation algorithms of lacustrine shale gas adsorption capacity: a case study of the Triassic strata in the southeastern Ordos basin, China," *International Journal of Coal Geology*, vol. 134-135, pp. 61–73, 2014.

[9] D. Feng and K. Xiao, "Constant velocity mercury injection and nuclear magnetic resonance in evaluation of tight sandstone reservoirs in western Sichuan basin," *Petroleum Geology&Experiment*, vol. 43, no. 2, pp. 368–376, 2021.

[10] H. Zhong, F. Zhang, Z. Zhao, C. Wei, and Y. Liu, "Micro-scale pore-throat distributions in tight sandstone reservoirs and its constrain to movable fluid," *Petroleum Geology&Experiment*, vol. 43, no. 1, pp. 77–85, 2021.

[11] J. Liu, X. Wu, H. Cui, Q. Gao, and K. Lei, "Influence factors of the movable fluid in the Shan 2 reservoirs of the Shanxi formation in the Yan'an area, Ordos basin," *Geology and Exploration*, vol. 57, no. 1, pp. 0231–0240, 2021.

[12] J. Yan, D. Qin, P. Wang, and H. Wang, "Occurrence characteristics and main controlling factors of movable fluid in tight sandstone reservoirs in Ordos basin," *Petroleum Geology and Recovery Efficiency*, vol. 27, no. 6, pp. 47–56, 2020.

[13] Y. Li, B. Guo, Z. Yang et al., "Reservoir characteristics and evaluation of tight sandstone of Triassic Yanchang formation Chang 6, submember of Madigou oil zone in Ordos basin," *Journal of Xi'an Shiyou University (Natural Science - Edition)*, vol. 35, no. 5, pp. 38–46, 2020.

[14] J. Huang, Y. Du, H. Wang et al., "Characteristics of micropore structure and movable fluid of extra-low permeability reservoir:a case study of lower Etl reservoir in A'er sag, Erlian basin," *Lithologic Reservoirs*, vol. 32, no. 5, pp. 93–101, 2020.

[15] T. Wang, H. Wei, W. Sun, J. Han, Y. Bai, and G. Gao, "Movable fluid traits and its main controlling factors in tight sandstone reservoir:taking Chang-6_3 of Huaging area in Ordos basin, China As an instance," *Unconventional Oi1&Gas*, vol. 7, no. 2, pp. 56–63, 2020.

[16] Z. Wang, "Microscopic pore structure and the seepage characteristics in tight sandstone reservoir of the 8th member of lower Shihezi formation in Linxing area of East Ordos basin," *Unconventional Oil & Gas*, vol. 7, no. 1, pp. 59–64, 2020.

[17] H. Huang, R. Li, W. Chen et al., "Revisiting movable fluid space in tight fine-grained reservoirs: a case study from Shahejie shale in the Bohai Bay basin, NE China," *Journal of Petroleum Science & Engineering*, vol. 207, article 109170, 2021.

[18] W. Ji, "Gas water relative flow of tight sandstone gas reservoirs and its influencing factors; case study of member 8 of Permian Xiashihezi formation and member 1 of Permian Shanxi formation in Shaan well 234-235 area of Sulige gas-field in Ordos basin," *Journal of Jilin University(Earth Science Edition)*, vol. 49, no. 6, pp. 1540–1551, 2019.

[19] S. Xie, W. Li, F. Leng, and X. Wang, "Distribution and controlling factors of movable fluid in tight sandstone reservoir: taking Chang 6 formation of Huaqing oilfield in Ordos basin as an example," *Geological Science and Technology Information*, vol. 38, no. 5, pp. 105–114, 2019.

[20] H. Huang, R. Li, F. Xiong et al., "A method to probe the pore-throat structure of tight reservoirs based on low- field NMR: insights from a cylindrical pore model," *Marine and Petroleum Geology*, vol. 117, no. 104344, p. 104344, 2020.

[21] H. Huang, R. Li, F. Z. Jiang, J. Li, and L. Chen, "Investigation of variation in shale gas adsorption capacity with burial depth: insights from the adsorption potential theory," *Journal of Natural Gas Science & Engineering*, vol. 73, no. 103043, p. 103043, 2020.

[22] S. Wu, S. Lin, D. Chao et al., "Fluid mobility evaluation based on pore structure investigation in tight sandstones:case study of Upper Triassic Chang 6 tight sandstones in Huaqing area, Ordos basin," *Natural Gas Geoscience*, vol. 30, no. 8, pp. 1222–1232, 2019.

[23] N. Liu, Z. Zhou, D. Ren, J. Nan, D. Liu, and Z. Du, "Distribution characteristics and controlling factors of movable fluid in tight sandstone gas reservoir: a case study of the eighth member of Xiashihezi formation and the first member of Shanxi formation in western Sulige gas field," *Lithologic Reservoirs*, vol. 31, no. 6, pp. 14–25, 2019.

[24] P. Li, W. Sun, C. Li, Y. L. Gao, Y. Y. Bai, and D. Kun, "Characteristics of movable fluids in the low permeability sandstone reservoir: taking the Chang 8 reservoir of Maling oilfield Ordos basin as an example," *Process in Geophysics*, vol. 33, no. 6, pp. 2394–2402, 2018.

[25] W. Hui, Y. Jia, F. Cheng, F. Liu, and D. Ren, "Impact of microscopic pore structure on moveable fluid saturation in He 8 reservoir of eastern Sulige gasfield," *Petroleum Geology and Recovery Efficiency*, vol. 25, no. 5, pp. 10–16, 2018.

[26] J. Gao, D. Ren, D. Liu, W. Sun, and J. Shi, "Impact of pore structures on features of movable fluid in tight sandstone reservoir:taking Chant 63 tight sandstone reservoir of Huaqing area in Ordos basin as an example," *Geological Science and Technology Information*, vol. 37, no. 4, pp. 184–189, 2018.

[27] S. Xiong, S. Chu, S. Pi, Y. He, S. Li, and Y. Zhang, "Micro-pore characteristics and recoverability of tight oil reservoirs," *Earth Science*, vol. 42, no. 8, pp. 1379–1385, 2017.

[28] C. Wu and X. Zhao, "Determination of T2 cut off value of nuclear magnetic resonance in tight sandstone reservoir and lower limit of movable fluid-a case study of Chang 9 reservoir of Wucangbao oilfield," *Unconventional Oiie&Gas*, vol. 4, no. 2, 2017.

[29] D. Liu, W. Sun, D. Ren, Q. Zhang, H. Ming, and B. Chen, "Features of pore-throat structures and movable fluid in tight gas reservoir: a case from the 8th member of Permian Xiashihezi formation and the 1st member of Permian Shanxi formation in the western area of Sulige Uasfield, Ordos basin," *Natural Gas Geoscience*, vol. 27, no. 12, pp. 2136–2146, 2016.

[30] L. Cao, W. Sun, J. Sheng, L. Huo, Q. Chen, and C. Xie, "A method to determine movable fluid saturation of low permeability and tight oil reservoirs-by taking tight oil reservoirs in sixth member of Yanchang formation in Banqiao area as an example," *Journal of Yangtze University (Natural Science Edition)*, vol. 13, no. 20, pp. 1–9, 2016.

[31] B. Liu, C. Tan, R. Li et al., "Study on the correlation between occurrence characteristics of movable fluids and microscopic pore structure of Chang 8 formation reservoir in central Ordos basin," *Fresenius Environmental Bulletin*, vol. 28, no. 4, pp. 3131–3140, 2019.

[32] B. Liu, C. Tan, R. Li, Y. Tan, G. Yu, and X. Lei, "Investigation of pore throat structure and fractal characteristic of tight sandstone of Chang 8 reservoir in Jiyuan area, Ordos basin," *Fresenius Environmental Bulletin*, vol. 28, no. 12, pp. 9865–9876, 2019.

[33] Z. Xu, Y. Wang, S. Jiang et al., "Impact of input, preservation and dilution on organic matter enrichment in lacustrine rift basin: a case study of lacustrine shale in Dehui depression of Songliao basin, NE China," *Marine and Petroleum Geology*, vol. 135, article 105386, 2022.

[34] Z. Xu, X. Li, J. Li et al., "Characteristics of source rocks and genetic origins of natural gas in deep formations, Gudian depression, Songliao basin, NE China," *ACS Earth and Space Chemistry*, vol. 6, no. 7, pp. 1750–1771, 2022.

[35] L. Tang, "Prediction model of oil-water relative permeability endpoint in extra-low permeability reservoir and numerical simulation: taking the 6-10 reservoir of middle Es3 in Pucheng as an example," *FAulT-Block Oil&Gas*, vol. 29, no. 1, pp. 78–82, 2022.